

# A high-precision Monte Carlo study of directed percolation in (1+1) and higher dimensions

Junfeng Wang<sup>1,2</sup>, Qingquan Liu<sup>1</sup> and Youjin Deng<sup>1</sup> \*

<sup>1</sup>*Hefei National Laboratory for Physical Sciences  
at Microscale and Department of Modern Physics,  
University of Science and Technology of China, Hefei 230027, China and*

<sup>2</sup>*School of Electronic Science and Applied Physics,  
Hefei University of Technology, Hefei 230009, China*

(Dated: January 3, 2019)

## Abstract

We present a Monte Carlo study of the bond and the site directed percolation model on the  $(d+1)$ -dimensional simple-cubic and the body-centered-cubic lattices with  $d = 2$  to 7, as well as on the square, triangular, honeycomb, and kagomé lattices for  $d = 1$ . With a cumulative-probability and a linking-hashing technique, the simulation is reasonably efficient, independent of  $d$ , and can be up to very large virtual lattices (e.g., more than  $10^{27}$  sites for  $d = 7$ ). A dimensionless ratio  $Q_{\mathcal{N}}$  is defined to locate the percolation threshold  $p_c$ . Universal scaling of  $Q_{\mathcal{N}}$  near  $p_c$  is checked, and accordingly the  $Q_{\mathcal{N}}$  data for systems in the same dimension are simultaneously analyzed by a formula, in which universal parameters occur only once. In comparison with existing results, our estimates for  $p_c$  are comparable or somewhat better for  $d = 1$ , and much more precise for  $d > 1$ . Extensive simulations are then carried out at the estimated thresholds. The probability distribution and the finite-size scaling of several quantities are studied. The critical exponents are accurately determined. At the upper critical dimensionality  $d_c = 4$ , logarithmic corrections are clearly observed and found to be well described by the theoretical predictions. For  $d > d_c$ , the mean-field behavior is confirmed.

PACS numbers: 64.60.ah, 05.70.Jk, 64.60.Ht

---

\* Email: yjdeng@ustc.edu.cn

## I. INTRODUCTION

Directed percolation (DP) is a geometric model generalized from ordinary (isotropic) percolation, first introduced by Broadbent and Hammersley (1957) [1]. It is a generalized percolation with a special direction along which activity can only propagate in one way but not the reverse [1–4]. This special direction is normally considered as the temporal direction while the others are spatial. It is widely agreed that a variety of phenomena in nature are related to DP, including epidemic disease [2], forest fire [1, 5], transport in porous media, etc. [3, 4].

As a typical non-equilibrium process, DP has attracted much attention from statistical physicists because of its simplicity and rich behavior [6–11]. Unfortunately, analytical solutions are scarce for DP, even in (1+1) dimensions. The direct experimental explorations are also difficult; until now, the exclusive example to our knowledge is the DP criticality in turbulent liquid crystals [12, 13]. This makes numerical means indispensable to study the DP process, which include series expansion, transfer matrix, Monte Carlo simulation, etc. Fruitful results have been obtained. By series expansion, Bleuse provided the first estimate of the percolation threshold  $p_c$  for bond DP on most of the typical lattices in  $(d + 1)$  dimensions with  $d = 1-7$  [14]. Essam and Jensen et al. gradually improved the precision for some (1+1)-dimensional lattices, both for bond and site DPs [15–22]. Similar progresses have been achieved in (2+1) and higher dimensions. Grassberger and Adler et al. improved the precision or established the first estimate of  $p_c$  for several lattices [23–28]. Among the existing results, the estimate of  $p_c$  on most of the (1+1)-dimensional lattices is impressively accurate; the uncertainty is at the *8th* decimal place. An exception is the site DP on the honeycomb lattice [18], of which the error margin is at the *6th* decimal place. In (2+1) and higher dimensions, the precision of  $p_c$  is less satisfactory.

Numerical methods like Monte Carlo simulation are usually limited to finite systems. Thus, theory of finite-size scaling (FSS) is widely used to extrapolate to infinite systems. Underlying FSS theory is the hypothesis of universality. It states that the singular critical behavior for various seemingly unrelated systems is governed by the same set of critical exponents. In equilibrium statistical mechanics, the universality hypothesis is supported by renormalization group (RG) theory. In this framework, critical systems of the same universality are in the same critical surface in the parameter space constructed by scaling

fields, and their scaling behavior is governed by a common fixed point. In two dimensions, beside numerical results, evidence for the universality hypothesis further arises from analytical calculations, conformal field theory, and Coulomb-gas theory. Compared to equilibrium statistical mechanics, less is known for non-equilibrium phase transition. This is due to the absence of an analog to equilibrium free energy and thus of a general treatment. Nevertheless, Janssen and Grassberger did propose a well-known universality hypothesis for DP [10, 11]: short-range interacting models, which exhibit a continuous phase transition into a unique absorbing state, belong to the DP universality class, if they have a one-component order parameter and no additional symmetries.

RG theory not only suggests the same set of critical exponents for systems in a universality class, but also implies universal scaling functions. In FSS theory, the linear system size is assumed to act as a scaling field with renormalization exponent  $-1$ , and thus FSS functions are also universal. Universal FSS behavior has been carefully checked for standard percolation and the Ising model, two paradigmatic systems in equilibrium statistical mechanics. However, for DP, less is known.

The FSS behavior of observables, such as specific heat and susceptibility in equilibrium system, is typically described by divergence according to power law modified by corrections to scaling. Thus, numerical treatment of the Monte Carlo data has to include both unknown critical exponents and unknown corrections. This introduces complications for data analysis and also restricts the accuracy of results. To overcome this difficulty, Binder introduced a dimensionless ratio  $U_4 = 1 - \langle m^4 \rangle / 3 \langle m^2 \rangle^2$  for the Ising model, where  $m$  is the magnetization density and  $\langle \rangle$  represents statistical average [29]. From universal FSS function, it can be shown that, if corrections to scaling are ignored, the  $U_4$  values for different system sizes are identical to a common value at the critical point, and further this common value is universal. The  $U_4$  data for different sizes typically display an approximately common intersection, which can be used to locate the critical point. Analogous universal ratios are widely used in systems besides the Ising model, and have been proved to be very powerful in numerically determining transition point [30].

In this work, we shall define a dimensionless ratio  $Q_{\mathcal{N}}$  for DP on the basis of the number of wet sites  $\mathcal{N}$ . It is observed that, as expected,  $Q_{\mathcal{N}}$  does obey universal FSS behavior for systems in the same universality. Further, as for equilibrium system, the dimensionless ratio  $Q_{\mathcal{N}}$  proves to be very useful in determining  $p_c$ . We then follow the strategy in Ref. [31] and

carry out a simultaneous analysis of systems in the same universality class, which include all site and bond DPs in the same dimension  $d$ . In such an analysis, all the Monte Carlo data with the same dimensionality  $d$  are combined together, and universal parameters occur only once in the fitting formula. This further improves our estimate of  $p_c$ . The underlying reason of the simultaneous analysis has been discussed in detail in Ref. [31], and shall be briefly mentioned. Finite-size data usually suffer from corrections to scaling. In the first order, these corrections are proportional to the leading irrelevant renormalization field, of which the amplitude approximately parameterizes the distance between the fixed point and the location of the model in the critical surface. Different systems in the same universality class usually have different amplitudes. A model with small irrelevant field can be well used to determine universal parameters like the critical ratio, but is not suitable to determine the irrelevant exponent. The well estimated universal ratio can help the Monte Carlo data for a model with a relatively large correction to determine the irrelevant exponent. Accordingly, the estimate of percolation threshold and other universal parameters is improved.

Extensive simulations were then carried out at the estimated percolation thresholds, and universal FSS functions of several quantities are studied. These include the wetting probability  $\mathcal{P}$ , the number of wet sites  $\mathcal{N}$ , and the mean gyration radius  $\mathcal{R}$ . To study their FSS functions, we measure the probability distribution (histogram) of these quantities. The critical exponents are determined, and the (hyper-)scaling relations are checked for  $d < d_c$ , where  $d_c = 4$  is the upper critical dimensionality. Logarithmic corrections at  $d = d_c$  are clearly observed and analyzed according to the theoretical calculation. For  $d > d_c$ , the hyperscaling relation breaks down and the mean-field prediction is confirmed.

The remainder of this paper is organized as follows. Section II briefly introduces the DP model, defines the lattices, and describes the algorithm. Results are presented in Secs. III and IV, which include the determination of the percolation thresholds and the study of the critical FSS behavior. A brief discussion is given in Sec. V.

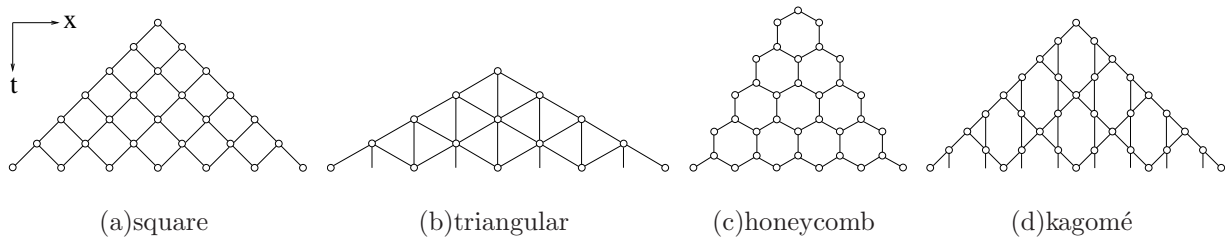


FIG. 1: Some (1+1)-dimensional lattices. The horizontal and vertical directions are regarded as the spatial and temporal directions, respectively.

## II. MODEL, LATTICE, AND ALGORITHM

### A. Model

Among various definitions of DP, the model of growing from a single wet site and the rule of parallel updating are adopted in this work. Consider the square lattice in Fig. 1(a), where the horizontal (vertical) direction is the spatial (temporal) direction. One starts with a single wet site at time  $t = 0$ . At each time step  $t$ , in the bond DP process, every edge, connecting an already-wet site at  $t$  and a lattice site at  $t + 1$ , becomes occupied with probability  $p$ ; sites at  $t + 1$  with one or more occupied edges are said to be wetted. In the site DP process, at each time step  $t$ , every lattice site at time  $t + 1$ , with one or more wet neighboring sites at  $t$ , is turned wetted with probability  $p$  (sites with no wet neighboring site at  $t$  cannot become wetted). For occupation probability  $p > 0$ , all the lattice sites in Fig. 1(a) can potentially be wetted, while those outside the geometry have no chance to get wetted.

For  $d \geq 1$ , there exist two distinct phases in the DP process. For small  $p$ , the number of wet sites  $\mathcal{N}(t)$  rapidly approaches to 0 as time  $t$  elapses, i.e., the propagation quickly dies out. For large  $p$ , the DP process becomes absorbed and  $\mathcal{N}(t)$  increases linearly as  $t^d$ . A phase transition point  $p_c$  occurs to separate these two phases. The number of wet sites  $\mathcal{N}(t)$  behaves as

$$\mathcal{N}(t) \propto \begin{cases} e^{-t/\xi_{\parallel}(p)} & p < p_c \\ t^{\theta} & p = p_c \\ t^d [a + O(e^{-t/\xi_{\parallel}(p)})] & p > p_c \end{cases} \quad (1)$$

where  $0 < a \leq 1$  accounts for the fraction of wet sites over the system. The correlation length  $\xi_{\parallel}$  in the temporal direction is a function of  $p$ , and diverges as  $\propto |p - p_c|^{-\nu_{\parallel}}$  when  $p \rightarrow p_c$ . The critical exponent  $0 \leq \theta < 1$  characterizes the scaling behavior of  $\mathcal{N}(t)$  at  $p_c$ .

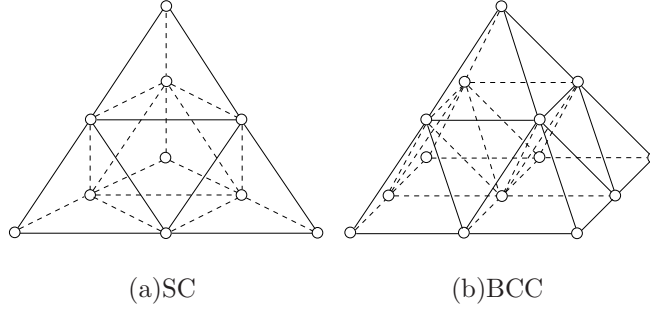


FIG. 2: (2+1)-dimensional SC and BCC lattices.

## B. Lattice

In (1 + 1) dimensions, besides the square lattice, we also study bond and site DPs on the triangular, honeycomb, and kagomé lattices. On the triangular lattice (Fig. 1(b)), at each time step  $t$ , the propagation of wet sites can be from time  $t$  to  $t + 1$  and from  $t$  to  $t + 2$ . On the honeycomb (Fig. 1(c)) and the kagomé lattice (Fig. 1(d)), the unit of temporal direction is defined such that the propagation occurs between time  $t$  and  $t + 1/2$  and between  $t + 1/2$  and  $t + 1$ .

For  $d = 2$  to 7, we study DP on the simple-cubic (SC) and the body-centered-cubic (BCC) lattice. On the SC lattice, each lattice site at time  $t$  has  $\lambda = d + 1$  neighboring sites at  $t + 1$ ; on the BCC lattice, one has  $\lambda = 2^d$ . Figure 2 shows the SC and BCC lattices in (2 + 1) dimensions. The visualization becomes difficult for  $d > 2$ , and we shall define the SC and the BCC lattice according to the association between a site at  $t$  and its neighboring sites at  $t + 1$ . This will be used in the actual Monte Carlo simulation. In  $(d + 1)$  dimensions, let  $\mathbf{v}_t \equiv (x_1, x_2, \dots, x_d)$  specify a lattice site at time  $t$ , where integer  $x_i \geq 0$  ( $i = 1, 2, \dots, d$ ) is the spatial coordinate. On the SC lattice, the coordinates of the  $\lambda = d + 1$  neighboring sites at  $t + 1$  are  $(x_1, x_2, \dots, x_d)$ ,  $(x_1 + 1, x_2, \dots, x_d)$ ,  $\dots$ ,  $(x_1, x_2, \dots, x_d + 1)$ , respectively. In other words, one of the  $\lambda = d + 1$  neighboring sites at time  $t + 1$  of  $\mathbf{v}_t$  has the same spatial coordinates as  $\mathbf{v}_t$ , while the others differ from  $\mathbf{v}_t$  by one lattice unit in one of the  $d$  directions. On the BCC lattice, the spatial coordinates of the  $\lambda = 2^d$  neighboring sites at time  $t + 1$  of  $\mathbf{v}_t$  read  $(x_1 \pm 1, x_2 \pm 1, \dots, x_d \pm 1)$ . Namely, the coordinate in each of the  $d$  spatial directions either increases or decreases by one lattice unit.

### C. Algorithm

As mentioned above, all lattice sites within the geometry in Figs. 1 and 2 have non-zero probability to get wetted. Thus, the number of the potentially wetted lattice sites  $V(t)$  increases approximately as  $a(t+1)^{d+1}$  as  $t$  elapses, with  $a > 0$  a constant. On the square, triangular, honeycomb, and kagomé lattices, constant  $a$  is  $1/2, 1/2, 1,$  and  $3/2,$  respectively; for the  $(d+1)$ -dimensional SC and BCC lattices, one has  $a \approx 1/(d+1)!$  and  $1/(d+1),$  respectively. Recording all these lattice sites would request a huge amount of computer memory for large  $t$  and  $d$ . Fortunately, this can be avoided in the DP process. When propagating from  $t$  to  $t+1$ , one only needs to know the locations of the wetted sites at  $t$ ; the unwetted sites are irrelevant in the propagation procedure. Thus, we introduce two first-in-first-out queues  $\mathbb{Q}_t$  and  $\mathbb{Q}_{t+1}$  to store the coordinates of the already-wet sites at  $t$  and of the unfinished list of wetted sites at  $t+1$  (for the triangular lattice, an additional queue  $\mathbb{Q}_{t+2}$  is needed), respectively. Each element of  $\mathbb{Q}$  is a  $d$ -dimensional vector  $\mathbf{v} \equiv (x_1, x_2, \dots, x_d),$  specifying the spatial coordinates of a lattice site. With these queues, the lattices in Figs. 1 and 2 are not directly stored in computer memory, and thus become “virtual”.

For large  $d$ , the percolation threshold  $p_c$  approximately equals to  $1/\lambda$ , and thus  $p_c$  is small for large  $d$ . Therefore, near the critical point, most of the lattice sites are unwetted, and storing the wetted sites instead of the whole virtual lattice would save numerous computer memory.

The small  $p_c$  also implies that many random numbers and many operations would be needed if all the potentially occupied edges (sites) are visited and determined whether or not they are occupied. The simulation efficiency would drop quickly as the coordination number  $\lambda$  increases. A more efficient procedure follows [32, 33]. Let  $\mathbf{v}_t$  be a wet site at  $t$ , one counts its  $\lambda$  neighboring sites sequentially, and defines  $P(k) \equiv (1-p)^{k-1}p$  to be the probability that the first  $(k-1)$  neighboring sites are empty (unwetted) while the  $k$ th site is wetted. The cumulative probability distribution  $C(k)$  is then

$$C(k) = \sum_{k'=1}^k P(k') = 1 - (1-p)^k. \quad (2)$$

Suppose the current wetted site is the  $k_0$ th neighbor of  $\mathbf{v}_t$ , one can obtain the next to-be-wetted site as the  $(k_0+k)$ th neighbor of  $\mathbf{v}_t$  by drawing a uniformly distributed random

number  $0 \leq r < 1$  and requesting

$$C(k-1) \leq r < C(k) . \quad (3)$$

The value of  $k$  can be obtained within  $\log_2(\lambda)$  steps by the standard bisection search method, which compares  $r$  to the value of the middle element of  $C(k)$  in the searching interval. Thus, instead of visiting all the potentially wetted sites, one can directly jump to the next to-be-wetted site. This step is repeated until all the neighboring sites of  $\mathbf{v}_t$  are visited—i.e.,  $k_0 + k > \lambda$ . By this way, the simulation efficiency is significantly improved for large  $d$ .

On this basis, one can formulate the algorithm as

**A.** Visit sites in queue  $\mathbb{Q}_t$  sequentially. For each site  $\mathbf{v}_t$  in  $\mathbb{Q}_t$ , starting with the  $k_0$ th neighbor of  $\mathbf{v}_t$  ( $k_0 = 0$  at the beginning),

**A.1** Calculate the location  $(k_0 + k)$  of the next to-be-wetted site  $\mathbf{v}_{t+1}$  by Eq. (3).

**A.2** Check if  $\mathbf{v}_{t+1}$  has already been wetted (visited) for bond (site) DP. If not, make  $\mathbf{v}_{t+1}$  wetted, and update queue  $\mathbb{Q}_{t+1}$ .

**A.3** Set  $k_0 \leftarrow k_0 + k$ . Repeat A.1 and A.2 until all the  $\lambda$  neighboring sites of  $\mathbf{v}_t$  are visited.

**B.** Repeat step A until all the elements in  $\mathbb{Q}_t$  are visited. Set  $\mathbb{Q}_t \leftarrow \mathbb{Q}_{t+1}$ .

The simulation continues until the aimed maximum time step  $t_{\max}$  is reached or the propagation dies out. In our Monte Carlo simulation, the maximum time  $t_{\max}$  is set in range  $2^{13} \leq t_{\max} \leq 2^{16}$ .

In the actual implementation, some difficulties may occur in step A.2. In this step, for bond DP, the main task is to check whether a to-be-wetted site (derived from Eq. (3)) is already wetted. For  $d=1$  and 2, this can be done easily by introducing an auxiliary “flag” to specify the wetted sites, since the memory is not yet a problem in modern computers typically of 2 GBytes or more. For  $d > 2$ , especially for large  $d$ , storing all lattice sites becomes impractical. In this case, as mentioned earlier, one introduces a to-be-complete queue  $\mathbb{Q}_{t+1}$  to store the wet sites only. When judging whether or not a to-be-wetted site  $\mathbf{v}_{t+1}$  should be added to the queue  $\mathbb{Q}_{t+1}$ , one may compare the coordinates of each already-in- $\mathbb{Q}_{t+1}$  site to those of  $\mathbf{v}_{t+1}$ , one by one. Such a comparison need about  $\langle N(t)^2 \rangle$  operations,

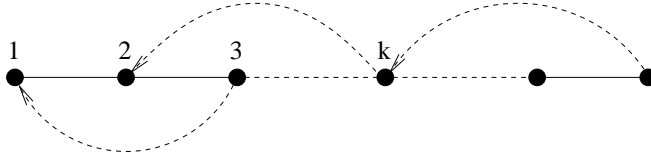


FIG. 3: Sketch of the linking-hashing technique. All elements in the same linked class have the same first two coordinates  $(x_1, x_2)$ . The linking direction is backward in queue  $\mathbb{Q}$ .

with  $N(t)$  is the number of wetted sites at time  $t$ . This effectively leads to a computational critical slowing-down.

We use a linking-hashing trick to resolve this difficulty. One classifies the sites in  $\mathbb{Q}_{t+1}$  by their first two coordinates  $(x_1, x_2)$ , and links all the sites with the same  $(x_1, x_2)$  by directed pointers. This is shown in Fig 3, where the pointer direction is backward (the sites at the head of the arrow are added to queue  $\mathbb{Q}_{t+1}$  earlier than the sites at tail). A hashing table  $\mathbb{H}(x_1, x_2)$  is introduced to store the top element of each class. With these auxiliary informations, the status-checking procedure can be done as following. When  $\mathbf{v}_{t+1}$  is derived, the linked class is immediately identified by its first two coordinates  $(x_1, x_2)$ , and the top element of the class is read out from table  $\mathbb{H}(x_1, x_2)$ . Then, along the directed linking, it is checked whether  $\mathbf{v}_{t+1}$  is identical to any site in this class. For completeness, we re-express step A.2 in the aforementioned algorithm as ‘A.2 Check if  $\mathbf{v}_{t+1}$  was already wetted (visited) for bond (site) DP. If not, make  $\mathbf{v}_{t+1}$  wetted, and update queue  $\mathbb{Q}_{t+1}$ , the linking, and the hashing table’.

At the percolation threshold  $p_c$ , the average number of wet sites scales as  $\mathcal{N}(t) \propto t^\theta$ . The scaling exponent  $\theta$  is in range  $0(d \geq 4) \leq \theta \leq 0.313686(d = 1)$ . More precisely, one has  $\mathcal{N}(t) \approx 1$  for  $d > 4$ —i.e., only a few wetted sites survive on the average. This means that the two-dimensional hashing table  $\mathbb{H}(x_1, x_2)$  is sparse and further that each linked class only contains a few sites. Thus, the status-checking procedure should be very efficient. Indeed, our simulation implies that, close to  $p_c$ , the CPU time for the status-checking procedure is of order  $O(1)$  per site, irrespective of the dimensionality  $d$ .

For site DP, one also sequentially visits the sites in queue  $\mathbb{Q}_t$  and generate via Eq. (3) the next to-be-wetted sites one by one. However, the status-checking procedure is slightly different from that for bond DP. The rule is more restrictive. A newly calculated to-be-wetted site  $\mathbf{v}_{t+1}$  cannot be added to queue  $\mathbb{Q}_{t+1}$  as long as it has already been visited,

irrespective of whether it was decided to be wetted or unwetted. Suppose  $\mathbf{v}_{t+1}$  is derived by Eq. (3) from the  $k$ th element in queue  $\mathbb{Q}_t$ , one observes that, if  $\mathbf{v}_{t+1}$  has already been visited, it must be a neighbor of some earlier element in  $\mathbb{Q}_t$  with label  $k' < k$ . In other words, no element in  $\mathbb{Q}_t$  with label  $k' < k$  can be a neighboring site of  $\mathbf{v}_{t+1}$ , if  $\mathbf{v}_{t+1}$  is to be wetted. This motivates us to classify the sites in  $\mathbb{Q}_t$  instead of  $\mathbb{Q}_{t+1}$ . Analogously, the classification is based on the first two coordinates of the elements in  $\mathbb{Q}_t$ , and all the elements in the same class are directly linked. When a to-be-wetted site  $\mathbf{v}_{t+1}$  is calculated by Eq. (3), all the linked classes, of which the elements in  $\mathbb{Q}_t$  may be neighboring to  $\mathbf{v}_{t+1}$ , are identified. Within these linked classes, it is checked whether there exists an element in queue  $\mathbb{Q}_t$  which is neighboring to site  $\mathbf{v}_{t+1}$ . If not,  $\mathbf{v}_{t+1}$  is added on the top of queue  $\mathbb{Q}_{t+1}$ , and the hashing table and the linking are updated. By this way, albeit a potentially wet site  $\mathbf{v}_{t+1}$  at  $t + 1$  may be visited several times and thus more than one random number is drawn, the status of  $\mathbf{v}_{t+1}$  is determined by the first drawn random number. The status-checking procedure is only slightly more complicate than for the bond DP, and thus the efficiency remains.

We mention that, near  $p_c$ , the maximum computer memory needed in simulation is not determined by the average size of the wetted sites at time  $t_{\max}$ . Instead, the maximum length of the queues  $\mathbb{Q}$  should be set as  $\propto t_{\max}^{y_N}$ , where the cut-off exponent  $y_N$  characterizes the wide-range probability distribution of the wet-site number  $\mathcal{N}(t)$ . Similarly, the hashing table  $\mathbb{H}(x_1, x_2)$  is of size  $\propto t_{\max}^{2y_R}$ , with the cut-off exponent  $y_R$  accounting for the probability distribution of the gyration radius  $\mathcal{R}$  of the wetted sites. It will be shown numerically that the cut-off exponents are in range  $0.4733(d = 1) \leq y_N \leq 1(d \geq 4)$  and  $0.63267(d = 1) \geq y_R \geq 1/2(d \geq 4)$ . In the actual implementation, it is monitored whether an overflow would occur in queues  $\mathbb{Q}$  and the hashing table  $\mathbb{H}$ .

We conclude this section by mentioning that a different hashing technique, using 64-bit integers, was applied to study the standard percolation and the DP in Refs. [34, 35].

### III. RESULT I: PERCOLATION THRESHOLD

Using the algorithm in Sec. II C, we study the bond and site DPs in  $(d+1)$  dimensions with  $d = 1-7$ . Preliminary and coarse simulations are performed for various  $p$  to approximately locate the percolation threshold  $p_c$  by looking at the intersection of a dimensionless ratio  $Q_N$  for different system sizes, which will be defined later. Then, fine and extensive simulations

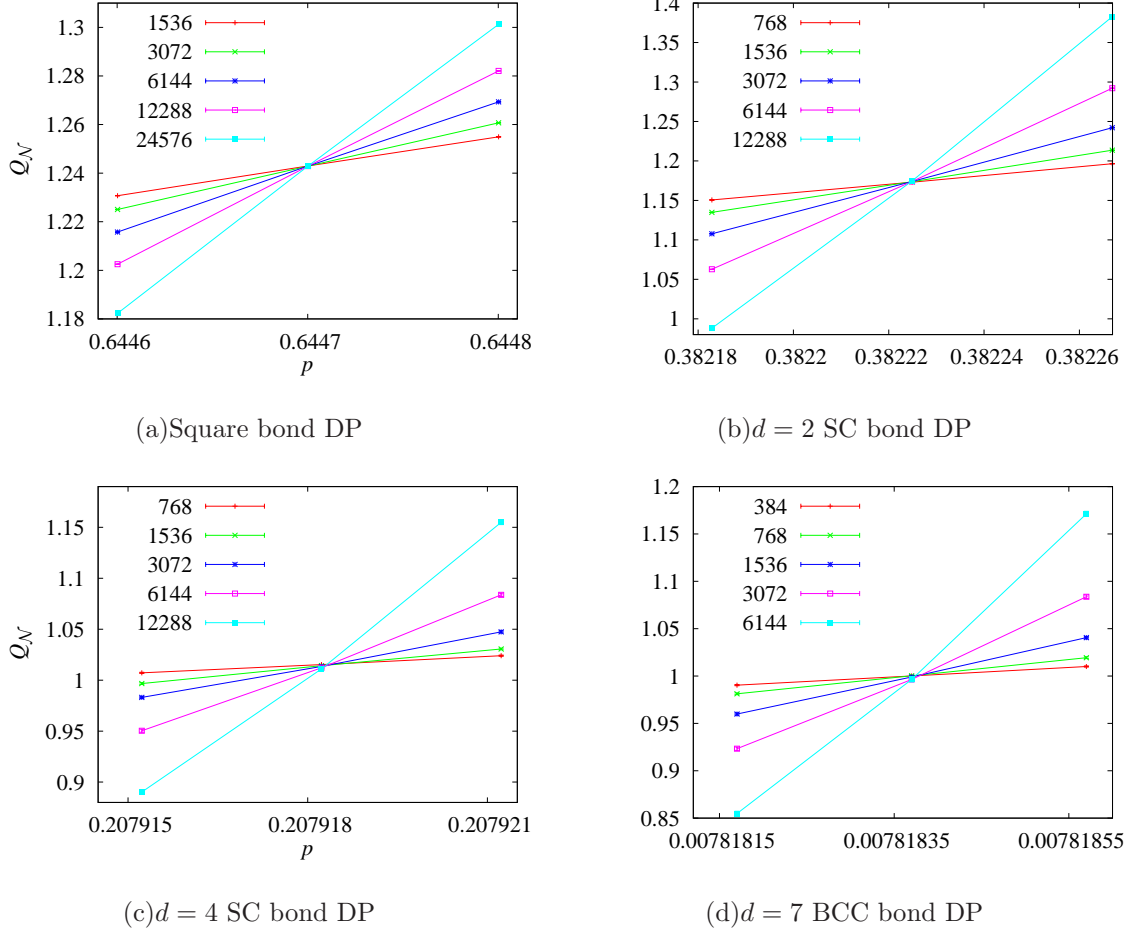


FIG. 4: Ratio  $Q_{\mathcal{N}}$  versus  $p$  for some DPs.

are carried out near the estimated critical point.

### A. Dimensionless ratio $Q_{\mathcal{N}}$

In the DP process, the number of wetted sites  $N(t)$  is recorded in computer memory for each time step  $t$ , and the statistical average  $\mathcal{N}(t) = \langle N(t) \rangle$  is calculated. An improved estimator of  $\mathcal{N}(t)$  was used in Refs. [34, 35], and found to reduce the variance of  $N(t)$  by a factor of about 3 for some unknown reason. In this work, we did not apply this improved estimator. To reduce the statistical fluctuation, we simply measure the average  $\overline{\mathcal{N}}$  in range  $(t, 2t]$  as

$$\overline{\mathcal{N}}\left(\frac{3t}{2}\right) = \frac{1}{t} \sum_{t'=t+1}^{2t} \mathcal{N}(t'), \quad (4)$$

where  $t$  is taken as  $t = 2^i$  with  $i = 1, \dots, i_{\max} - 1$ . Apparently,  $\overline{\mathcal{N}}(t)$  at the percolation threshold  $p_c$  behaves the same as  $\mathcal{N}(t)$ —i.e.,  $\overline{\mathcal{N}}(t) \propto t^\theta$ .

As discussed in the Introduction, in equilibrium statistical mechanics, universal dimensionless ratios are found to be very powerful in locating critical point. Therefore, we also define for DP a dimensionless ratio as

$$Q_{\mathcal{N}}(t) = \overline{\mathcal{N}}(2t)/\overline{\mathcal{N}}(t) . \quad (5)$$

According to the scaling behavior of  $\overline{\mathcal{N}}(t)$ , we expect: (1), for  $p < p_c$ , the  $Q_{\mathcal{N}}(p, t)$  value quickly approaches to 0 as  $t$  increases, (2), for  $p > p_c$ , it rapidly reaches  $2^d$ , and (3), at  $p = p_c$ , it converges to the universal value  $2^\theta$ . The  $Q_{\mathcal{N}}$  data versus  $p$  for different time steps  $t$  should display an intersection, which indicates the percolation threshold  $p_c$ . This is indeed the case, and some results are shown in Fig. 4. A rough eye-view fitting yields  $p_c = 0.644\ 70(1)$  for the square-lattice bond DP,  $p_c = 0.382\ 222(1)$  for the  $d = 2$  SC bond DP,  $p_c = 0.207\ 918(1)$  for the  $d = 4$  SC bond DP, and  $p_c = 0.007\ 818\ 3(1)$  for the  $d = 7$  BCC bond DP. The estimate of  $p_c$  for the  $d = 4$  SC bond DP falsifies the existing result  $p_c = 0.208\ 5(2)$ .

Mod	$Q_c$	$y_p$	$y_u$	$q_1$	$q_2$	$q_2/q_1^2$	$b_1$
S <sup>b</sup>	1.2428(1)	0.5764(6)	-0.98(3)	-1.747(8)	-1.05(7)	-0.34(3)	0.54(6)
S <sup>s</sup>	1.2429(1)	0.5775(7)	-1.05(4)	-1.632(7)	-0.91(3)	-0.34(2)	0.52(4)
T <sup>b</sup>	1.24287(8)	0.575(1)	-0.90(8)	-1.679(6)	-0.99(9)	-0.35(4)	0.4(2)
T <sup>s</sup>	1.24292(8)	0.577(1)	-1.05(9)	-1.41(2)	-0.9(3)	-0.5(2)	0.39(7)
H <sup>b</sup>	1.24290(8)	0.578(2)	-1.02(3)	-2.68(4)	-2.5(2)	-0.35(4)	1.0(2)
H <sup>s</sup>	1.2429 (1)	0.5758(5)	-1.01(1)	-2.77(2)	-2.7(2)	-0.35(4)	0.8(1)
K <sup>b</sup>	1.24291(6)	0.577(1)	-0.99(2)	-2.17(2)	-1.4(3)	-0.30(7)	0.25(3)
K <sup>s</sup>	1.2429 (1)	0.576(1)	-0.96(2)	-2.18(2)	-1.6(1)	-0.34(3)	0.26(2)

TABLE I: Result from the separate fits of  $Q_{\mathcal{N}}$  in (1+1) dimensions. Superscripts  $b$  and  $s$  represent the bond and site DPs, respectively.

According to renormalization group theory, the behavior of the wet-site number  $\mathcal{N}(p, t)$ , and thus of the dimensionless ratio  $Q_{\mathcal{N}}$ , obeys a universal scaling function near  $p_c$  for all

S <sup>b</sup>	S <sup>s</sup>	T <sup>b</sup>	T <sup>s</sup>
0.644 700 1(2)	0.705 485 3(3)	0.478 025 0(4)	0.595 646 9(2)
H <sup>b</sup>	H <sup>s</sup>	K <sup>b</sup>	K <sup>s</sup>
0.822 856 9(2)	0.839 931 6(2)	0.658 968 9(2)	0.736 931 7(2)

TABLE II: Estimate of  $p_c$  from the separate fits of  $Q_{\mathcal{N}}$  in (1+1) dimensions.

DPs in the same universality class. In other words, we expect that

$$Q_{\mathcal{N}}(p, t) = \tilde{Q}_{\mathcal{N}}(vt^{y_p}, ut^{y_u}), \quad (|p - p_c| \ll p_c) \quad (6)$$

where  $v$  and  $u$  represent the amplitudes of the relevant and leading irrelevant scaling fields, respectively, and  $y_p = 1/\nu_{\parallel}$  and  $y_u < 0$  are the associated renormalization exponents. Function  $\tilde{Q}_{\mathcal{N}}$  and exponents,  $y_p$  and  $y_u$ , are universal. The amplitude  $u$  characterizes the distance between the fixed point and the location of a critical system in the critical surface, and is thus model-dependent. The relevant scaling field  $v$  can be expanded in the occupation probability  $p$ , as

$$v = a_j(p_{cj} - p_j) + e_j(p_{cj} - p_j)^2 + \dots \quad (7)$$

where  $p_{cj}$  is the percolation threshold for the  $j$ th DP model. The coefficients  $a_j$  and  $e_j$  are nonuniversal constants.

In order to bring Eq. (6) in a suitable form to describe the Monte Carlo data for  $Q_{\mathcal{N}}(p, t)$ , the universal function  $\tilde{Q}_{\mathcal{N}}$  can be Taylor-expanded as

$$\tilde{Q}_{\mathcal{N}} = Q_c + t^{y_p} v_j Q_1 + t^{2y_p} v_j^2 Q_2 + \dots + u_j t^{y_u} + \dots, \quad (8)$$

where the amplitude  $Q_i$ , obtained from the  $i$ th derivative of  $\tilde{Q}_{\mathcal{N}}$ , is also universal. The universal value  $Q_c$  relates to exponent  $\theta$  as  $Q_c = 2^{\theta}$ .

## B. Separate analysis

*Result for  $d = 1$ .* For  $d = 1$ , extensive simulations were carried out for the bond and site DPs on the square (S), triangular (T), honeycomb (H), and kagomé (K) lattices, which include 8 models in total. The maximum time step is set as  $t_{\max} = 2^{16}$  for all these 8 models, which corresponds to virtual lattices of  $\approx 10^9$  sites. For each system, about  $10^9$  samples are

taken. The simulation runs on a cluster of 128 CPUs and takes about 12 years of CPU time for a PC of 2.66GHz frequency.

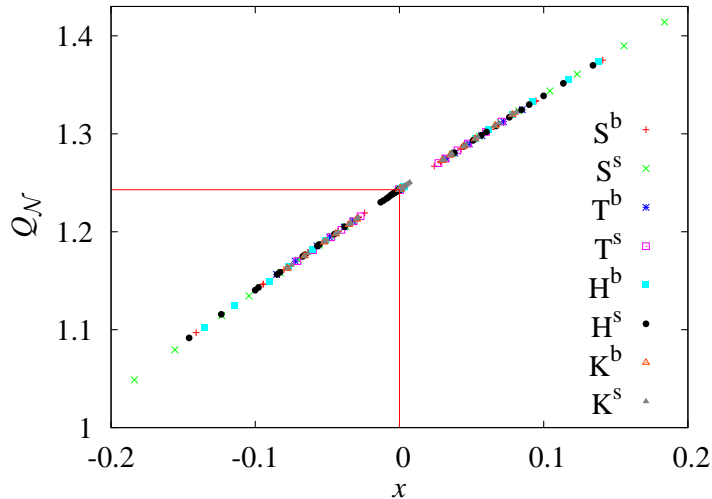


FIG. 5: Ratio  $Q_{\mathcal{N}}$  versus parameter  $x$  for DPs with  $d = 1$ . Parameter  $x$  is calculated as  $x = q_{1j}(p_{cj} - p_j)t^{y_p}$ , with  $q_{1j}$  and  $p_{cj}$  taken from Tables. I and II. The excellent collapse indicates the universality class.

According to a least-squared criterion, the  $Q_{\mathcal{N}}(p, t)$  data are fitted by

$$Q_{\mathcal{N}} = Q_c + q_{1j}(p_{cj} - p_j)t^{y_p} + q_{2j}(p_{cj} - p_j)^2 t^{2y_p} + q_{3j}(p_{cj} - p_j)^3 t^{3y_p} + c_j(p_{cj} - p_j)t^{y_p+y_u} + b_{1j}t^{y_u} + b_{2j}t^{y_2}, \quad (9)$$

which is obtained by substituting Eq. (7) in Eq. (8) and ignoring high-order nonlinear and correction terms. For simplicity, the second correction exponent  $y_2$  is fixed at  $y_2 = -2$ . In the fit, the Monte Carlo data for  $t < t_{\min}$  are excluded, where  $t_{\min}$  is gradually increased until the residual  $\chi^2$  is comparable to the degrees of freedom (d.f.) and the  $\chi^2$  value does not drops significantly when a few more data points are thrown away. Furthermore, analogous fitting procedures are carried out by excluding those poorly-determined terms or including additional terms in Eq. (9). Consistency and stability of the results are checked. The error margins are estimated by taking into account the statistical errors directly from the fits and the variation in different fits. The estimated error bars are taken so that they can at least cover the fitting results from different fits.

The results are shown in Tables. I and II. Universality is confirmed by the good agreement of the universal ratio  $Q_c$  and the exponent  $y_p$  for all the 8 models. We also compute

Model	$Q_c$	$y_p$	$y_u$	$q_1$	$q_2$	$q_2/q_1^2$	$b_1$
SC <sub>2</sub> <sup>b</sup>	1.1734(1)	0.7762(5)	–	-3.15(1)	2.65(5)	0.267(7)	–
SC <sub>2</sub> <sup>s</sup>	1.1737(4)	0.7767(7)	-0.46(8)	-2.42(1)	1.56(1)	0.266(4)	-0.022(6)
BCC <sub>2</sub> <sup>b</sup>	1.1735(2)	0.7758(3)	–	-4.20(1)	4.70(5)	0.266(5)	–
BCC <sub>2</sub> <sup>s</sup>	1.1729(4)	0.7761(6)	-0.58(7)	-2.92(2)	2.28(3)	0.267(8)	0.027(5)
SC <sub>3</sub> <sup>b</sup>	1.0774(6)	0.905(4)	–	-3.90(4)	6.4(2)	0.42(3)	–
SC <sub>3</sub> <sup>s</sup>	1.077(2)	0.904(7)	-0.33(5)	-2.67(6)	3.2(2)	0.45(5)	0.028(5)
BCC <sub>3</sub> <sup>b</sup>	1.0762(5)	0.902(5)	–	-8.36(8)	30(1)	0.43(3)	–
BCC <sub>3</sub> <sup>s</sup>	1.077(2)	0.901(5)	-0.37(3)	-5.0(1)	11.4(4)	0.46(4)	0.034(2)
SC <sub>4</sub> <sup>b</sup>	1.007(7)	0.984(7)	-0.20(6)	-4.34(7)	10.4(6)	0.54(5)	0.031(6)
SC <sub>4</sub> <sup>s</sup>	1.011(4)	0.983(8)	-0.28(7)	-2.9(3)	4.6(6)	0.5(2)	0.059(3)
BCC <sub>4</sub> <sup>b</sup>	1.007(3)	0.984(3)	-0.16(5)	-15.0(3)	126(7)	0.56(6)	0.016(2)
BCC <sub>4</sub> <sup>s</sup>	1.011(5)	0.975(9)	-0.30(6)	-9.6(9)	43(8)	0.5(2)	0.059(3)
SC <sub>5</sub> <sup>b</sup>	1.000(2)	0.999(7)	-0.45(9)	-5.2(3)	15(3)	0.6(2)	0.025(9)
SC <sub>5</sub> <sup>s</sup>	1.000(2)	0.997(5)	-0.47(4)	-4.2(1)	11(2)	0.6(2)	0.052(5)
BCC <sub>5</sub> <sup>b</sup>	1.0000(3)	1.001(3)	-0.45(7)	-30.9(7)	566(37)	0.59(7)	0.0075(7)
BCC <sub>5</sub> <sup>s</sup>	0.9994(6)	1.005(9)	-0.41(8)	-21(2)	235(33)	0.5(2)	0.04(1)
SC <sub>6</sub> <sup>b</sup>	0.9998(5)	0.993(4)	-0.8(3)	-6.8(3)	26(3)	0.6(2)	0.021(9)
SC <sub>6</sub> <sup>s</sup>	0.9999(5)	0.998(4)	-0.9(2)	-5.4(2)	16(1)	0.55(8)	0.05(1)
BCC <sub>6</sub> <sup>b</sup>	0.9999(4)	0.999(5)	-0.9(4)	-64(2)	2539(192)	0.62(9)	0.0018(5)
BCC <sub>6</sub> <sup>s</sup>	0.9999(5)	1.003(4)	-0.9(2)	-48(2)	1280(90)	0.56(9)	0.05(2)
SC <sub>7</sub> <sup>b</sup>	0.9997(3)	1.000(4)	-1.3(5)	-7.6(2)	33(3)	0.57(9)	0.014(5)
SC <sub>7</sub> <sup>s</sup>	0.9996(7)	1.003(4)	-1.2(2)	-6.4(2)	24(2)	0.59(9)	0.040(8)
BCC <sub>7</sub> <sup>b</sup>	1.0000(2)	1.002(4)	-0.9(2)	-126(4)	10032(1344)	0.6(2)	0.0005(2)
BCC <sub>7</sub> <sup>s</sup>	1.0000(2)	0.997(4)	-1.1(1)	-108(3)	6698(900)	0.6(1)	0.034(8)

TABLE III: Result from the separate fits of  $Q_{\mathcal{N}}$  for DPs with  $d = 2-7$ . Superscripts  $b$  and  $s$  are for the bond and site DPs, respectively, and subscript denotes the spatial dimensionality  $d$ . Symbol “–” means that the corresponding parameter cannot be well determined, since the error margin is comparable or larger than the absolute value of the parameter itself; thus, the corresponding term is not included in the fit.

$d$	SC <sup>b</sup>	SC <sup>s</sup>	BCC <sup>b</sup>	BCC <sup>s</sup>
2	0.382 224 66(6)	0.435 314 3(1)	0.287 338 38(6)	0.344 573 86(9)
3	0.268 356 38(10)	0.303 395 52(9)	0.132 374 19(3)	0.160 961 31(10)
4	0.207 918 20(7)	0.231 046 98(8)	0.063 763 404(7)	0.075 585 18(1)
5	0.170 615 20(4)	0.186 513 61(5)	0.031 456 634(2)	0.035 972 52(2)
6	0.145 089 92(4)	0.156 547 20(4)	0.015 659 387(6)	0.017 333 055(5)
7	0.126 387 50(4)	0.135 004 21(4)	0.007 818 373(3)	0.008 432 989(3)

TABLE IV: Estimate of  $p_c$  from the separate fits of  $Q_N$  for DPs with  $d = 2-7$ .

$q_2/q_1^2$ , which is equal to  $Q_2/Q_1^2$ . It can be seen that the  $q_2/q_1^2$  values are also identical for different systems, supporting the statement that Eq. (6) is universal. To further demonstrate the universality, we plot the  $Q_N(p, t)$  data for all these DPs versus parameter  $x$ , where  $x = q_{1j}(p_{cj} - p_j)t^{y_p}$  is calculated from Tables. I and II. The excellent collapse is observed in Fig. 5, where the data for the small time step  $t < 1536$  are excluded in order to avoid the influence from finite-size corrections.

The fits for all the 8 models give the leading correction exponent as  $y_u \approx -1$ . The estimates of  $p_c$  are already quite precise, of which the error margins are at the 7th decimal place.

*Result for  $d = 2$  and 3.* The simulation for  $d = 1$  and 2 did not use the linking-hashing technique, or the cumulative-probability trick. For  $d > 2$  these two tricks improves the efficiency and limits the used computer memory. For the BCC lattice in  $(7 + 1)$  dimensions, the coordination number is  $\lambda = 2^d = 128$ ; no significant decreases of the efficiency is observed.

There exist 24 systems for the site and bond DPs on the SC and BCC lattices for  $d = 2-7$ . For the majority of these systems, the maximum time step is set at  $t_{\max} = 2^{13}$ ; for the others,  $t_{\max}$  is larger than  $2^{13}$ . For each of these systems, about  $10^9$  samples are taken. The total CPU time is about 43 years for a PC with 2.66GHz frequency.

Following the similar procedure for  $d = 1$ , the  $Q_N$  data are fitted by Eq. (9). The results are shown in Tables. III and IV. The determinations of  $Q_c$ ,  $y_p$ , and  $q_{2j}/q_{1j}^2$  agree well with each other for all the DPs in the same spatial dimension. Moreover, in two and three dimensions, the  $Q_c = 2^\theta$  value clearly deviates from 1, implying the critical exponent  $\theta \neq 0$ .

The estimate of  $p_c$  is rather good, the precision of which already exceeds that of the existing results. However, it is rather difficult to determine the leading correction exponent  $y_u$ . For the bond DP, the  $Q_{\mathcal{N}}$  data can be described by Eq. (9) without including the correction term with exponent  $y_u$ ; this is represented by symbol “–” in Table III. If such a term is included, the amplitude  $b_1$  and the associated error margin are of the same magnitude. For the site DP, we determine the correction exponent as  $y_u \approx -0.50(d=2)$  and  $-0.35(d=3)$ .

*Result for  $d = 4$ .* The upper critical dimensionality for the DP universality class is believed to be  $d_c = 4$ . For  $d > d_c$ , the mean-field prediction becomes valid and the critical behavior is governed by the Gaussian fixed point in renormalization group theory, which yields the renormalization exponent  $1/\nu_{\parallel} = 1$  and  $\theta = 0$ . Nevertheless, at  $d = d_c = 4$ , the existence of dangerous irrelevant scaling fields typically leads to both multiplicative and additive logarithmic corrections for finite-size scaling.

Despite of the possible existence of logarithmic correction, as a crude analysis we also fitted the  $Q_{\mathcal{N}}$  data by Eq. (9). The results are shown in Tables III and IV. While slowly convergent corrections with exponent  $y_u \approx -0.2$  are observed in most cases, the  $Q_{\mathcal{N}}$  data for the bond DP on the BCC lattice do not suffer from severe finite-size corrections. The estimates of  $Q_c$  and  $y_p$  agree more or less with the mean-field prediction  $Q_c = 1$  and  $y_p = 1/\nu_{\parallel} = 1$ , albeit significant deviations can indeed be observed for some cases. From these deviations, it seems that multiplicative logarithmic corrections with negative exponent exist in terms associated with  $y_p$ .

For  $d = d_c$ , the leading and subleading logarithmic corrections have been calculated by Janssen and Stenull from field theory [36], and are partially confirmed by Monte Carlo simulation [35]. At critical point, the scaling behavior of the average wet-site number  $\mathcal{N}(t)$  is described by [36]

$$\mathcal{N}(t) = N_0 \left[ \ln \frac{t}{t_0} - b \ln \ln \frac{t}{t_1} + a \right]^{\alpha} \quad (10)$$

where the known quantities are  $\alpha = 1/6$ ,  $b = 1.30204$ , and  $a = 0.1831$ , and unknown constants  $N_0$ ,  $t_0$  and  $t_1$  are model-dependent. It is further predicted [37] that, if only the leading logarithmic corrections are taken into account,  $\mathcal{N}(p, t)$  behaves as

$$\mathcal{N}(p, t) \approx (\ln t)^{\alpha_1} \Phi_{\mathcal{N}}(t(\ln t)^{\alpha_2} \Delta p) \quad (11)$$

where  $\Phi_{\mathcal{N}}$  is a universal scaling function and the exponents are  $\alpha_1 = 1/6$  and  $\alpha_2 = -1/6$ .

Accordingly, we fit the  $\mathcal{N}(p, t)$  data by

$$\mathcal{N}(p, t) = (\ln t + h_1)^{\alpha_1} \times \left[ q_0 + \sum_{k=1}^3 q_k (p_c - p)^k t^k (\ln t + h_2)^{k\alpha_2} + b_1 t^{y_1} + b_2 t^{y_2} \right], \quad (12)$$

with  $y_1 = -1$  and  $y_2 = -2$  fixed. Indeed, the  $\mathcal{N}(p, t)$  data can be well described by Eq. (12) with  $\alpha_1 = 1/6$  and  $\alpha_2 = -1/6$  being fixed; the results for  $h_1$  and  $h_2$  are shown in Table V. If  $h_1$  and  $h_2$  are fixed at the values in Table V, the exponents  $\alpha_1$  and  $\alpha_2$  can be determined

Model	SC <sub>4</sub> <sup>b</sup>	SC <sub>4</sub> <sup>s</sup>	BCC <sub>4</sub> <sup>b</sup>	BCC <sub>4</sub> <sup>s</sup>
$h_1$	0.6(2)	-1.27(20)	3.4(2)	-1.1(2)
$h_2$	2.1(6)	-2.2(7)	3.2(6)	-2.0(5)

TABLE V: Estimate of  $h_1$  and  $h_2$  in Eq. (12), with  $\alpha_1 = 1/6$  and  $\alpha_2 = -1/6$  being fixed.

as in Table VI, in agreement with the theoretical values. Nevertheless, the present Monte Carlo data do not allow the simultaneous determination of  $\alpha_i$  and  $h_i$  ( $i = 1, 2$ ).

Model	SC <sub>4</sub> <sup>b</sup>	SC <sub>4</sub> <sup>s</sup>	BCC <sub>4</sub> <sup>b</sup>	BCC <sub>4</sub> <sup>s</sup>	Ref [37]
$\alpha_1$	0.171(8)	0.167(4)	0.165(3)	0.166(5)	1/6
$\alpha_2$	-0.17(2)	-0.17(2)	-0.16(2)	-0.16(2)	-1/6

TABLE VI: Estimate of  $\alpha_1$  and  $\alpha_2$  in Eq. (12), with  $h_1$  and  $h_2$  fixed at the values in Table V.

We also fit the  $Q_{\mathcal{N}}(p, t)$  data by

$$Q_{\mathcal{N}} = Q_c \left( 1 + \frac{\ln 2}{\ln t + h_1} \right)^{\alpha_1} + c_j (p_c - p) t^{y_p + y_u} (\ln t + h_2)^{\alpha_2} + \sum_{k=1}^3 q_k (p_c - p)^k t^{ky_p} (\ln t + h_2)^{k\alpha_2} + b_1 t^{y_1} + b_2 t^{y_2}, \quad (13)$$

where  $\alpha_1 = 1/6$ ,  $\alpha_2 = -1/6$ ,  $y_1 = -1$ ,  $y_2 = -2$  are fixed. To estimate  $Q_c$  and  $y_p$ , we took the values of  $h_1$  and  $h_2$  in Table. V. The results are shown in Table VII; the estimates of  $Q_c$  and  $y_p$  are now consistent with the mean-field predictions. With  $Q_c = 1$  and  $y_p = 1$  being fixed, the estimate of the percolation threshold is  $p_c(\text{SC}_4^b) = 0.207\,918\,18(4)$ ,  $p_c(\text{SC}_4^s) = 0.231\,046\,87(4)$ ,  $p_c(\text{BCC}_4^b) = 0.063\,763\,395(4)$ , and  $p_c(\text{BCC}_4^s) = 0.075\,585\,16(2)$ , in good agreement with those in Table IV.

Model	$Q_c$	$y_p$	$q_1$	$q_2$	$q_2/q_1^2$	$b_1$
SC <sub>4</sub> <sup>b</sup>	1.0002(4)	1.002(7)	-5.50(8)	16(2)	0.53(9)	-0.15(4)
SC <sub>4</sub> <sup>s</sup>	1.0000(5)	1.004(4)	-3.48(6)	6.4(4)	0.52(6)	-0.6(2)
BCC <sub>4</sub> <sup>b</sup>	0.9999(2)	1.000(2)	-19.6(2)	216(10)	0.56(4)	-0.06(4)
BCC <sub>4</sub> <sup>s</sup>	1.0003(7)	1.003(3)	-10.3(2)	55(4)	0.52(6)	-0.05(2)

TABLE VII: Result of the separate analysis for  $d = 4$ , according to Eq. (13).

*Result for  $d = 5, 6$ , and  $7$ .* For  $d > d_c = 4$ , the critical behavior of DP should be described by mean-field theory, which yields the renormalization exponent  $y_p = 1/\nu_{\parallel} = 1$  and  $\theta = 0$ . This implies that, on average, the wet-site number  $\mathcal{N}(t) \propto t^{\theta} = 1$  is just of a few sites, independent of the propagation time. It will be shown later that, at  $d = d_c$ , one has  $\mathcal{N}(t) \approx 1.2$  up to  $t = 10^4$ .

The  $Q_{\mathcal{N}}$  data are fitted by Eq. (9), and the results are shown in Tables III and IV. The mean-field predictions  $Q_c = 2^{\theta} = 1$  and  $y_p = 1$  are well confirmed. The estimated values  $q_2/q_1^2$  are identical for all the site and bond DPs on different lattices and in different dimensions. The leading correction exponent is  $y_u \approx -1/2$  for  $d = 5$  and  $y_u \approx -1$  for  $d = 6$  and  $7$ . We suspect that  $y_u(d = 5) \approx -1/2$  is due to the crossover phenomena arising from the small distance to the upper critical dimensionality. The determination of the percolation threshold is up to the 8th or even the 9th decimal place, reflecting the efficiency of our algorithm.

### C. Simultaneous analysis

The results of Sec. III B indicate that, as expected, the FSS behavior of observables near the critical point is indeed described by universal scaling function for systems in the same universality class. For the present work, this means that all the DPs in the same dimension  $d$  are in the same universality class; the number of different systems is 8 for  $d = 1$  and 4 for  $d > 1$ . Assuming that the universality strictly holds and thus the universal parameters are exactly the same, we combine the  $Q_{\mathcal{N}}(p, t)$  data for all the DPs with the same  $d$  and analyze them simultaneously by a single formula, in which the universal parameters only occur once.

Separating the universal from the nonuniversal constants in Eqs. (7) and (8) yields

$$\begin{aligned}
Q_{\mathcal{N}} = & Q_c + Q_1 a_j (p_{cj} - p_j) t^{y_p} + Q_2 a_j^2 (p_{cj} - p_j)^2 t^{2y_p} + Q_3 a_j^3 (p_{cj} - p_j)^3 t^{3y_p} \\
& + c_j (p_{cj} - p_j) t^{y_p + y_u} + b_{1j} t^{y_u} + b_{2j} t^{y_u^2},
\end{aligned} \tag{14}$$

where  $Q_c$ ,  $Q_i$  ( $i = 1, 2, 3$ ),  $y_p$ , and  $y_u$  are universal.

$d$	$Q_c$	$Q_2$	$Q_3$	$y_p$	$y_u$
1	1.24293(5)	-0.33(1)	-0.29(1)	0.5766(2)	-1.03(3)
2	1.17346(13)	0.266(2)	-0.041(8)	0.7758(4)	-0.52(4)
3	1.0769(2)	0.441(4)	0.09(3)	0.9033(16)	-0.39(2)
4	1.0075(7)	0.544(8)	0.24(3)	0.983(3)	-0.22(3)
5	1 (fixed)	0.56(2)	–	1 (fixed)	-0.48(2)
6	1 (fixed)	0.56(2)	–	1 (fixed)	-0.95(8)
7	1 (fixed)	0.57(2)	0.37(9)	1 (fixed)	-1.12(6)

TABLE VIII: Result for the universal parameters from the simultaneous fit of  $Q_{\mathcal{N}}$ .

Lattice	Site		Bond	
	$p_c$ (Present)	$p_c$ (Known)	$p_c$ (Present)	$p_c$ (Known)
square	0.705 485 25(9)	0.705 485 22(4) [20]	0.644 700 19(5)	0.644 700 185(5) [20]
		0.705 489(4) [21]		0.644 700 15(5) [19]
triangular	0.595 646 86(8)	0.595 646 75(10) [22]	0.478 025 26(9)	0.478 025 25(5) [22]
		0.595 646 8(5) [19]		0.478 025(1) [19]
honeycomb	0.839 931 70(5)	0.839 933(5) [18]	0.822 856 90(4)	0.822 856 80(6) [22]
kagomé	0.736 931 75(8)	0.736 931 82(4) [22]	0.658 969 03(7)	0.658 969 10(8) [22]

TABLE IX: Estimated percolation threshold  $p_c$  of the DPs in (1+1) dimensions, obtained from the simultaneous fit of  $Q_{\mathcal{N}}$ .

Following the similar procedure as in Sec. IIIB, the  $Q_{\mathcal{N}}(p, t)$  data near  $p_c$  are fitted by Eq. (14) according to the least-squared criterion. Note that, in Eq. (14), the universal parameter  $Q_1$  and the model-dependent constants  $a_j$  are not independent parameters and

Lattice	Site		Bond	
	$p_c(\text{Present})$	$p_c(\text{Known})$	$p_c(\text{Present})$	$p_c(\text{Known})$
(2+1)-d SC	0.435 314 19(6)	0.435 31(7) [24]	0.382 224 64(4)	0.382 223(7) [24]
(2+1)-d BCC	0.344 573 98(6)	0.344 573 6(3) [28]	0.287 338 38(4)	0.287 338 3(1) [25]
		0.344 575(15) [27]		0.287 338(3) [24]
(3+1)-d SC	0.303 395 54(5)	0.302 5(10) [26]	0.268 356 32(4)	0.268 2(2) [14]
(3+1)-d BCC	0.160 961 23(3)	0.160 950(30) [27]	0.132 374 21(2)	not found
(4+1)-d SC	0.231 046 94(3)	not found	0.207 918 19(2)	0.208 5(2) [14]
(4+1)-d BCC	0.075 585 173(6)	0.075 585 0(3) [28]	0.063 763 402(3)	not found
		0.075 582(17) [27]		
(5+1)-d SC	0.186 513 57(4)	not found	0.170 615 18(3)	0.171 4(1) [14]
(5+1)-d BCC	0.035 972 547(8)	0.035 967(23) [27]	0.031 456 634(1)	not found
(6+1)-d SC	0.156 547 22(2)	not found	0.145 089 95(3)	0.145 8 [14]
(6+1)-d BCC	0.017 333 055(3)	not found	0.015 659 385(3)	not found
(7+1)-d SC	0.135 004 21(2)	not found	0.126 387 51(2)	0.127 0(1) [14]
(7+1)-d BCC	0.008 432 989(2)	not found	0.007 818 373 0(8)	not found

TABLE X: Estimated percolation threshold  $p_c$  of the DPs in  $(d+1)$  dimensions with  $d = 2-7$ , obtained from the simultaneous analysis of  $Q_{\mathcal{N}}$ .

thus cannot be both determined in the analysis. We set  $Q_1 = 1$  in the fit, which defines a scale of the relevant field. The results are summarized in Tables VIII-X. For DPs above the upper critical dimensionality  $d_c = 4$ , the mean-field predictions,  $Q_c = 1$  and  $y_p = 1$ , are well confirmed if  $Q_c$  and  $y_p$  are left as free parameters to be determined by the fit. Thus, we only present in Tables VIII-X the results with  $Q_c = 1$  and  $y_p = 1$  being fixed. It is suggested that the  $Q_2$  value is identical to a single value for  $d > d_c$ , and thus the  $Q_{\mathcal{N}}$  data for all the DPs for  $d > d_c$  can be in principle combined together and analyzed simultaneously. For simplicity, we did not carry out such an analysis.

At  $d_c = 4$ , the results  $Q_c = 1.0075(7)$  and  $y_p = 0.983(3)$  clearly deviate from the mean-field values  $Q_c = 1$  and  $y_p = 1$ , due to logarithmic corrections. Thus, we fit the  $Q_{\mathcal{N}}$  data

by

$$Q_{\mathcal{N}} = Q_c \left( 1 + \frac{\ln 2}{\ln t + h_{1j}} \right)^{\alpha_1} + c_j (p_{cj} - p_j) t^{y_p + y_u} (\ln t + h_{2j})^{\alpha_j} + \sum_{k=1}^3 Q_k a_j^k (p_{cj} - p_j)^k t^{ky_p} (\ln t + h_{2j})^{\alpha_2} + b_{1j} t^{y_1} + b_{2j} t^{y_2}, \quad (15)$$

where  $\alpha_1 = 1/6$ ,  $\alpha_2 = -1/6$ ,  $y_1 = -1$ ,  $y_2 = -2$ ,  $Q_c = 1$  and  $y_p = 1$  are fixed. The determined percolation thresholds,  $p_c(\text{SC}_4^b) = 0.20791818(3)$ ,  $p_c(\text{SC}_4^s) = 0.23104688(4)$ ,  $p_c(\text{BCC}_4^b) = 0.063763395(3)$ ,  $p_c(\text{BCC}_4^s) = 0.07558515(1)$ , agree well with those in Table X.

Compared to the separate analysis, the precision of  $p_c$  and of universal parameters is significantly improved. A comparison of the threshold  $p_c$  with the existing results is presented in Tables IX and X. In (1+1) dimension, our determination of  $p_c$  agrees with the existing results, with a comparable or somewhat better precision. These  $d = 1$  results are mostly obtained by series expansions. We consider it valuable to provide an independent study by a distinct method. For  $d > 2$ , Monte Carlo simulation turns out to be an efficient method. Our results for  $d = 2-7$  provide a number of first estimates of  $p_c$  or a significant improvement on the precision of  $p_c$ .

Finally, let us discuss the  $p_c$  values given in Table X for  $d \geq 2$ . In terms of coordination number  $\lambda$ , Kurrer et al. suggested an empirical formula [38],

$$1/p_c \approx a_1 + a_2 \lambda, \quad (16)$$

where  $a_i$  ( $i=1, 2$ ) are some unknown constants. The formula (16) applies for large  $\lambda$ , and cannot describe the  $p_c$  values for small  $\lambda$ . In Fig. 6, we plot the  $1/p_c$  value versus  $\lambda$ . It is interesting to observe that the slopes are approximately identical for the bond and site DPs on the SC lattice, while on the BCC lattice they clearly have different slopes. We take the  $d = 6$  and 7 data, and calculate  $a_1$  and  $a_2$  according to Eq. (16). The results are shown in Table XI. On this basis, we suspect: (1), the  $a_2$  value is not necessary equal to 1, and (2),

	SC <sup>b</sup>	SC <sup>s</sup>	BCC <sup>b</sup>	BCC <sup>s</sup>
$a_1$	-0.2470	-0.7474	-0.1849	-3.1954
$a_2$	1.0199	1.0193	1.0007	0.9514

TABLE XI: Estimate of  $a_1$  and  $a_2$  in Eq. (16), calculated from the  $d = 6$  and 7 data.

the  $a_2$  value is identical for the bond and the site DP on the SC lattice.

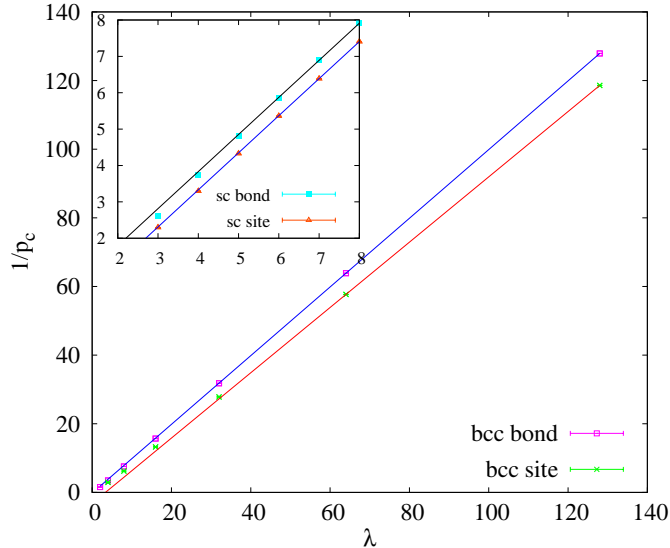


FIG. 6:  $1/p_c$  versus coordination number  $\lambda$  for the bond and the site DP on the BCC lattice. The lines are obtained by Eq. (16) according to the  $d = 6$  and  $7$  data. The inset displays for the SC lattice.

#### IV. RESULT II: SCALING AT CRITICALITY

*Sampled quantities and scaling behavior.* To study the scaling behavior of other quantities, we simulate the bond DP on square and higher-dimensional BCC lattices with  $d$  from 2 to 5, at  $p_c = 0.644\,700\,185$  ( $d = 1$ ),  $0.287\,338\,38$  ( $d = 2$ ),  $0.132\,374\,21$  ( $d = 3$ ),  $0.063\,763\,404$  ( $d = 4$ ), and  $0.031\,456\,633$  ( $d = 5$ ), which are, within the error margin, at the estimated critical points in Tables IX and X. Besides the wet-site number  $N(t)$ , we sample the wetting probability  $P(t)$  and a revised gyration radius  $R(t)$ . The wetting probability  $P(t)$  accounts for the probability that, at time  $t$ , the DP propagation still survives. Namely,  $P(t) = 1$  represents that there is at least one wetting site at time  $t$ , while  $P(t) = 0$  is for no wetting site. The revised gyration radius  $R(t)$  is defined as

$$R(t) = \begin{cases} 0 & N(t) = 0 \\ \sqrt{R_S(t)^2/N(t)} & N(t) \geq 1 \end{cases} \quad \text{with} \quad R_S(t)^2 = \sum_{i=1}^{N(t)} |\mathbf{v}_i|^2, \quad (17)$$

where  $|\mathbf{v}_i|$  is the modulus of the spatial coordinates of site  $i$ . On the basis of  $P(t)$ ,  $N(t)$ ,

and  $R(t)$ , we measure

$$\begin{aligned}\mathcal{P}(t) &= \langle P(t) \rangle \\ \mathcal{N}(t) &= \langle N(t) \rangle, \quad \mathcal{N}_k(t) = \langle N(t)^k \rangle, \\ \mathcal{R}(t) &= \langle R(t) \rangle, \quad \mathcal{R}_k(t) = \langle R(t)^k \rangle,\end{aligned}\tag{18}$$

with  $k = 2, 3, 4$ . Note that  $\mathcal{R}(t)$  is different from the traditional definition

$$\mathcal{R}_T(t)^2 = \langle R_S(t)^2 \rangle / \langle N(t) \rangle = \mathcal{R}_2(t) / \mathcal{P}(t).\tag{19}$$

In Monte Carlo simulation, the revised gyration radius  $\mathcal{R}(t)$  is a directly measured observable, while the traditional radius  $\mathcal{R}_T(t)$  is a composite quantity.

At critical point  $p_c$ , it is already known that the scaling behavior of  $\mathcal{P}(t)$ ,  $\mathcal{N}(t)$ , and  $\mathcal{R}_T(t)$  is

$$\mathcal{P}(t) \propto t^{-\delta}, \quad \mathcal{N}(t) \propto t^\theta, \quad \text{and} \quad \mathcal{R}_T(t) \propto t^{1/z},\tag{20}$$

where critical exponent  $z$  characterizes the anisotropy between the temporal and the spatial direction. Let  $\nu_{\parallel}$  and  $\nu_{\perp}$  denote the exponents describing the behavior of the correlation lengths along the temporal and the spatial directions, respectively,  $\xi_{\parallel} \propto |p - p_c|^{-\nu_{\parallel}}$  and  $\xi_{\perp} \propto |p - p_c|^{-\nu_{\perp}}$ , one has  $z = \nu_{\parallel} / \nu_{\perp}$ . From Eqs. (17) and (19), it can be derived that, at criticality, the revised gyration radius  $\mathcal{R}(t)$  behaves as

$$\mathcal{R}(t) \propto \mathcal{P}(t) \mathcal{R}_T(t) \propto t^{-\delta+1/z}.\tag{21}$$

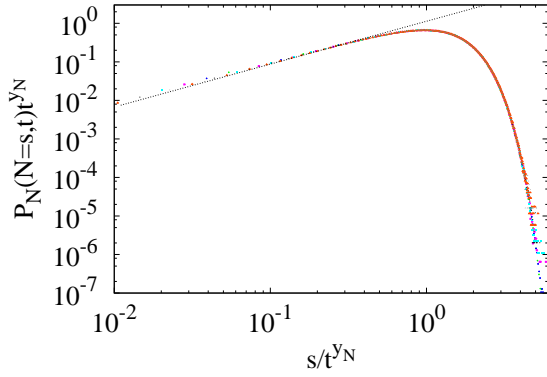
Analogously, it is expected that, at criticality, the higher-order moments of the wet-site number  $N(t)$  and of the revised gyration radius  $R(t)$  behave as

$$\mathcal{N}_k(t) \propto t^{y_{N_k}} \quad \text{and} \quad \mathcal{R}_k(t) \propto t^{y_{R_k}}, \quad (k = 2, 3, 4).\tag{22}$$

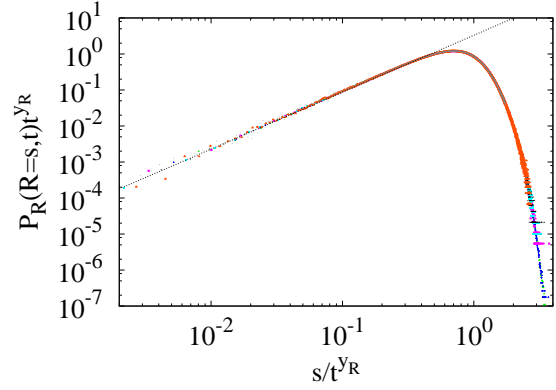
*Probability distribution.* We further examine the probability distribution of  $N(t)$  and  $R(t)$ . For simplicity, we consider the conditional probability that there is at least one wet site. More precisely, we define  $\mathbb{P}_N(N = s, t)$  as the probability that, conditioning on that the DP propagation still survives,  $N(t)$  is equal to given number  $s$ . The same applies to the conditional probability  $\mathbb{P}_R(R = s, t)$  of  $R(t)$ .

According to FSS theory, together with the Monte Carlo data, we assume that the probability distributions,  $\mathbb{P}(N = s, t)$  and  $\mathbb{P}(R = s, t)$ , are described by

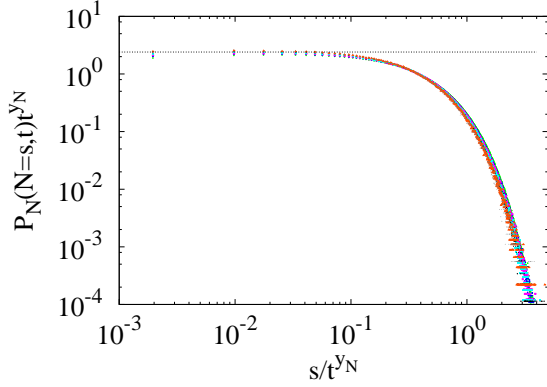
$$\mathbb{P}_N(N = s, t) \propto t^{-y_N} F_N(s/t^{y_N}), \quad \mathbb{P}_R(R = s, t) \propto t^{-y_R} F_R(s/t^{y_R}),\tag{23}$$



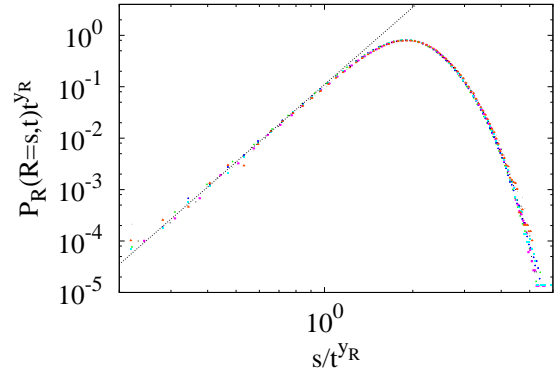
(a)  $\mathbb{P}_N$  for  $d = 1$



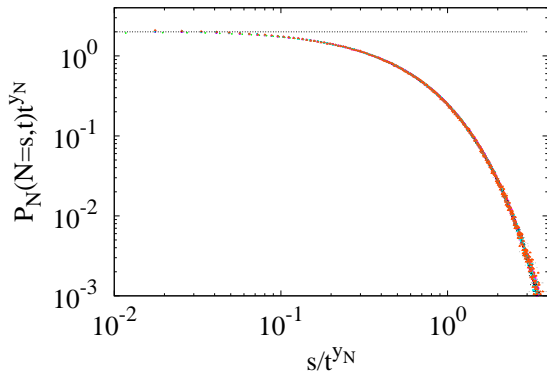
(b)  $\mathbb{P}_R$  for  $d = 1$



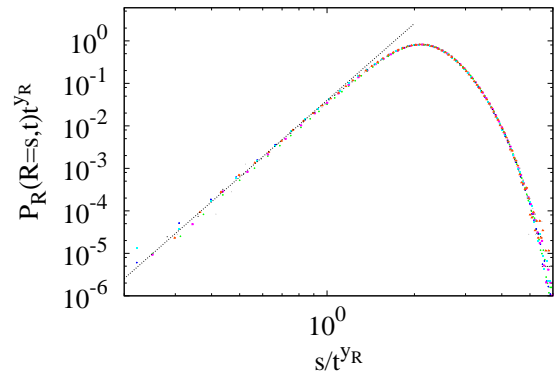
(c)  $\mathbb{P}_N$  for  $d = 4$



(d)  $\mathbb{P}_R$  for  $d = 4$



(e)  $\mathbb{P}_N$  for  $d = 5$



(f)  $\mathbb{P}_R$  for  $d = 5$

FIG. 7: Probability distributions  $\mathbb{P}_N$  and  $\mathbb{P}_R$ . The exponents  $y_N$  and  $y_R$  are taken from Table XII. The time steps are  $t = 2048, 4096, \dots, 131072$  for  $d=1$ ,  $t = 512, 1024, \dots, 32768$  for  $d=4$ , and  $t = 256, 512, \dots, 16384$  for  $d=5$ . The slope of the dashed straight line is  $1/y_N - 1$  for  $\mathbb{P}_N$  and  $1/y_R - 1 + d$  for  $\mathbb{P}_R$ .

each involves only one critical exponent,  $y_N$  or  $y_R$ . Functions,  $F_N$  and  $F_R$ , are expected to be universal. Figure 7 displays  $\mathbb{P}_N t^{y_N}$  ( $\mathbb{P}_R t^{y_R}$ ) versus  $s/t^{y_N}$  ( $s/t^{y_R}$ ) for  $d = 1, 4$  and  $5$ . The exponents are set to be  $y_N = 0.4733$  and  $y_R = 0.63267$  for  $d = 1$ , as numerically determined latter. For  $d = 4$  and  $5$ , the mean-field predictions  $y_N = 1$  and  $y_R = 1/2$  are used. A good collapse is observed. Theoretically, for  $d = d_c = 4$ , Eq. (29) suggests a better collapse should occur for  $\mathbb{P}_N t Y^{-\frac{1}{3}} \sim s/(t Y^{-\frac{1}{3}})$  and  $\mathbb{P}_R t^{\frac{1}{2}} Y^{\frac{1}{24}} \sim s/(t^{\frac{1}{2}} Y^{\frac{1}{24}})$ . Nevertheless, no significant improvement is observed in the eye view.

The dashed lines in Fig. 7 have slope  $1/y_N - 1$  for  $\mathbb{P}_N$  and  $1/y_R - 1 + d$  for  $\mathbb{P}_R$ . The approximate collapse of the line and the numerical data indicates that for small  $s$ , the universal functions  $F_N$  and  $F_R$  behave as a power law, as typical in critical phenomena. Accordingly, it seems that one can rewrite Eq. (23) as

$$\begin{aligned}\mathbb{P}_N(N = s, t) &\propto t^{-1} s^{1/y_N - 1} f_N(s/t^{y_N}) \\ \mathbb{P}_R(R = s, t) &\propto t^{-1 - d y_R} s^{1/y_R - 1 + d} f_R(s/t^{y_R}),\end{aligned}\quad (24)$$

where  $f_N(s/t^{y_N})$  and  $f_R(s/t^{y_R})$  are universal.

From the probability distribution (23), it can be derived that

$$\begin{aligned}\mathcal{N}(t) &\propto t^{-\delta + y_N}, & \mathcal{N}_k(t) &\propto t^{-\delta + k y_N} \\ \mathcal{R}(t) &\propto t^{-\delta + y_R}, & \mathcal{R}_k(t) &\propto t^{-\delta + k y_R}.\end{aligned}\quad (25)$$

Comparing Eq. (25) to Eqs. (20) and (21), one obtains the relations

$$y_N = \theta + \delta, \quad \text{and} \quad y_R = 1/z. \quad (26)$$

As well known, for DP there exist only three independent exponents, which are usually chosen as  $\beta$ ,  $\nu_{\parallel}$ , and  $\nu_{\perp}$ . The others can be obtained by scaling relations [6]

$$\delta = \beta/\nu_{\parallel}, \quad z = \nu_{\parallel}/\nu_{\perp}, \quad \text{and} \quad \theta = (d\nu_{\perp} - 2\beta)/\nu_{\parallel}, \quad (27)$$

where the last one involves the spatial dimensionality  $d$  and is usually referred to as the hyper-scaling relation. In this work, for the convenience of finite-size scaling, we choose  $y_p$ ,  $y_R$  and  $\delta$  as the three independent exponents. Then, the other exponents can be obtained as

$$\begin{aligned}\nu_{\parallel} &= 1/y_p, & z &= 1/y_R, & \nu_{\perp} &= y_R/y_p, \\ \theta &= d y_R - 2\delta, & \beta &= \delta/y_p, & y_N &= d y_R - \delta.\end{aligned}\quad (28)$$

At  $d = d_c = 4$ , the scaling behavior (25) is modified by multiplicative logarithmic factor. From the calculations by Janssen and Stenull [36], it can be derived that a power-law behavior normally becomes

$$t^x \rightarrow t^{x_{\text{m.f.}}} \left[ \ln \frac{t}{t_0} - b \ln \ln \frac{t}{t_1} + a_x \right]^{\alpha_x} \equiv t^{x_{\text{m.f.}}} Y^{\alpha_x}, \quad (29)$$

where  $x$  is some critical exponent, and  $x_{\text{m.f.}}$  represents the mean-field value. Amplitude  $b$  is universal and equal to  $b = 1.30204$ ,  $t_0$  and  $t_1$  are unknown integration constants from the renormalization-group flow, which are model-dependent but observable-independent, and  $a_x$  is observable-dependent. One further knows that

$$\begin{aligned} \delta_{\text{m.f.}} &= 1, \quad \alpha_\delta = -1/2, \quad \text{and} \quad \theta_{\text{m.f.}} = 0, \quad \alpha_\theta = 1/6, \\ y_{N,\text{m.f.}} &= 1, \quad \alpha_{y_N} = -1/3, \quad \text{and} \quad y_{R,\text{m.f.}} = 1/2, \quad \alpha_{y_R} = 1/24. \end{aligned} \quad (30)$$

On this basis, we have

$$\begin{aligned} \mathcal{P}(t) &= \mathcal{P}_0 t^{-1} Y^{1/2}, \\ \mathcal{N}(t) &= \mathcal{N}_0 t^0 Y^{1/6}, \quad \mathcal{N}_k(t) = \mathcal{N}_{k0} t^{k-1} Y^{(3-2k)/6}, \\ \mathcal{R}(t) &= \mathcal{R}_0 t^{-1/2} Y^{13/24}, \quad \mathcal{R}_k(t) = \mathcal{R}_{k0} t^{(k-2)/2} Y^{(12+k)/24}. \end{aligned} \quad (31)$$

In order to numerically confirm Eq. (31), we plot the critical  $\mathcal{N}(t)$ ,  $\mathcal{P} \cdot t$ , and  $\mathcal{R}_2$  data for the  $d = 4$  BCC bond DP in Fig. 8(a-c), respectively; the leading behavior of these quantities is expected by the logarithmic factor. Amplitude  $a$  in Eq. (29) is known as 0.1831 for  $\mathcal{N}$ ,  $-1.5193$  for  $\mathcal{P} \cdot t$  [36]. With  $a = 0.1831$  and  $\alpha_\theta = 1/6$  being fixed, the analysis of the  $\mathcal{N}$  data yields  $t_0 \approx 0.0072$ ,  $t_1 \approx 0.037$  and  $N_0 \approx 0.8119$ . Since  $t_0$  and  $t_1$  are observable-independent for given system, they are fixed in the analysis of the  $\mathcal{P} \cdot t$  and  $\mathcal{R}_2$  data. The results are shown in Fig. 8(a-c). For comparison, the data at  $p = 0.063763318$  and  $0.063763490$  are also shown. The clear deviation from the theoretical prediction for large  $t$  implies that they are indeed respectively in the dilute and the absorbing phase in the DP process. One also expects that, from Eq.(31), the logarithmic factors  $Y$  in product  $\mathcal{N}\mathcal{N}_2/t$  would cancel out and thus  $\mathcal{N}\mathcal{N}_2/t$  rapidly approaches to a constant as  $t$  increases. In Fig. 8(d), we plot  $\mathcal{N}\mathcal{N}_2/t - 0.11t^{-0.25}$  versus  $t$ , where  $-0.11t^{-0.25}$  is obtained from the fit and the small exponent  $-0.25$  is probably due to logarithmic correction.

*Determination of critical exponents.* From the Monte Carlo data at criticality, we aim to numerically determine the critical exponents  $\delta$ ,  $\theta$ ,  $z$ ,  $y_N$ ,  $y_R$ , etc. Besides  $\mathcal{P}(t)$ ,  $\mathcal{N}(t)$ , and  $\mathcal{R}(t)$ , we also analyze  $\mathcal{N}_k(t)$ ,  $\mathcal{R}_k(t)$ ,  $\mathcal{N}_k(t)/\mathcal{N}_{k-1}(t)$  and  $\mathcal{R}_k(t)/\mathcal{R}_{k-1}(t)$  with  $k \geq 2$ .

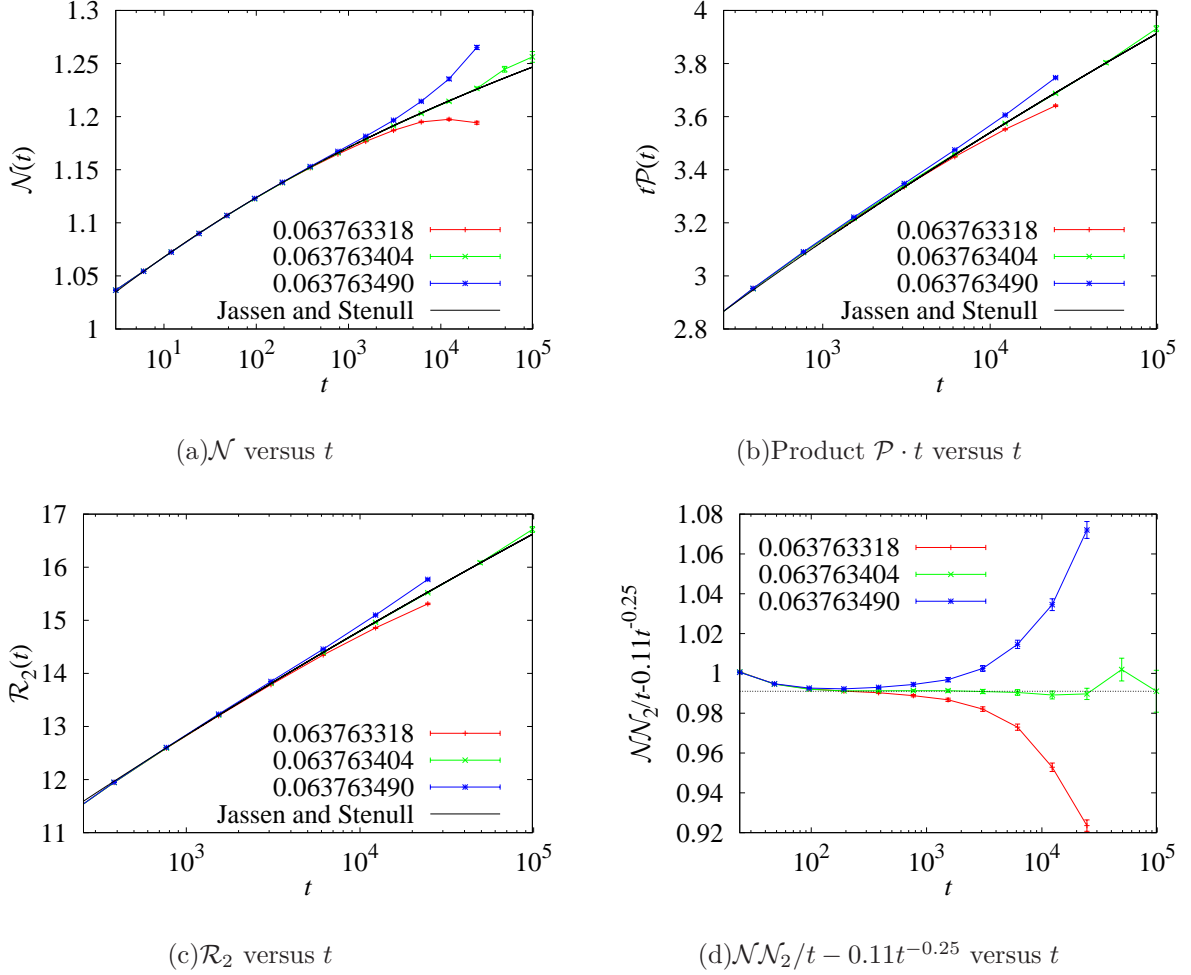


FIG. 8: Plot of various quantities for the (4+1)-dimensional BCC bond DP. The analytical curves in (a-c) are calculated from Eq. (31) with the unknown parameter obtained from the fits. The dashed line in (d) is just for guiding eyes.

To reduce one more unknown parameter in the fitting formula, we measure dimensionless ratios as following

$$\begin{aligned}
Q_P(t) &= \frac{\mathcal{P}(2t)}{\mathcal{P}(t)} & Q_N(t) &= \frac{\mathcal{N}(2t)}{\mathcal{N}(t)} & Q_R(t) &= \frac{\mathcal{R}(2t)}{\mathcal{R}(t)} \\
Q_{N_k} &= \frac{\mathcal{N}_k(2t)}{\mathcal{N}_k(t)} & Q_{R_k} &= \frac{\mathcal{R}_k(2t)}{\mathcal{R}_k(t)} \\
D_{N_k} &= \frac{\mathcal{N}_k(2t)\mathcal{N}_{k-1}(t)}{\mathcal{N}_k(t)\mathcal{N}_{k-1}(2t)} & D_{R_k} &= \frac{\mathcal{R}_k(2t)\mathcal{R}_{k-1}(t)}{\mathcal{R}_k(t)\mathcal{R}_{k-1}(2t)} \quad (k = 2, 3, 4), \quad (32)
\end{aligned}$$

which are fitted by

$$Q = Q_c + b_1 t^{y_u} + b_2 t^{y_2} + b_3 t^{y_3}, \quad (33)$$

with  $y_2 = -2$ ,  $y_3 = -3$ . In comparison with Eq. (9), all the  $p$ -dependent terms are absent

since it is at critical point. For  $d = d_c$ , taking into account the logarithmic corrections, we have the formula as

$$Q = Q_c \left(1 + \frac{\ln 2}{\ln t + h}\right)^\alpha + b_1 t^{y_1} + b_2 t^{y_2} + b_3 t^{y_3}, \quad (34)$$

where  $\alpha$  can be obtained from Eq. (31) and  $y_1 = -1$ .

From the estimate of  $Q_c$ , we calculate the associated exponent from the relation  $Q_c = 2^x$ . For example, the fit of the  $Q_{\mathcal{P}}(d = 1)$  data gives  $Q_{c,\mathcal{P}} = 0.89537(1)$ , which yields  $\delta = -\ln Q_{c,\mathcal{P}}/\ln 2 = 0.15944(2)$ . The same applies to other quantities. The results are shown in Tables XII and XIII; the latter is for the  $\delta$  result. The symbol “\*” for  $d = 4$  represents that the results are from the fits with logarithmic correction.

All the exponents shown in Table XII are mutually self-consistent. Further, the scaling relation, Eq. (26), is well confirmed. For  $d \leq d_c = 4$ , the hyper-scaling relation in Eq. (28) also holds.

On the basis of Tables VIII and XII, we calculate other critical exponents from the scaling relations (28). Note that we directly take  $y_N - \delta$  in Table XII as our estimate of exponent  $\theta$  instead of calculating it by  $\theta = dy_R - 2\delta$ , avoiding further error propagation. The estimates of these critical exponents, together with the existing results, are shown in Table XIII. For  $d = 1$ , our results are consistent with the existing result but worse than the latter. For  $d = 2, 3$ , our estimate significantly improves over the existing results by a factor from 4 to 10. For  $d = d_c = 4$ , the results with the logarithmic corrections agree well with the mean-field predictions. For  $d = 5$ , the mean-field values are confirmed.

## V. CONCLUSIONS

We present a systematic and high-precision Monte Carlo study of the bond and site directed percolations on  $(d + 1)$ -dimensional lattices with  $d$  from 1 to 7. In order to obtain accurate results, the simulation of large time-steps is necessary. However, due to the restriction of computer memory, the large-time-step simulation is notoriously difficult. We formulate an efficient algorithm by adopting the cumulative-probability and the linking-hashing technique. This allows us to obtain high-precision Monte-Carlo data within reasonable computing source.

A dimensionless ratio  $Q_{\mathcal{N}}$  is defined and used to determine the percolation threshold

$d + 1$	$y_{N-\delta}$	$2y_{N-\delta}$	$3y_{N-\delta}$	$4y_{N-\delta}$	$y_N(D_{N_2})$	$y_N(D_{N_3})$	$y_N(D_{N_4})$
	$y_{R-\delta}$	$2y_{R-\delta}$	$3y_{R-\delta}$	$4y_{R-\delta}$	$y_R(D_{R_2})$	$y_R(D_{R_3})$	$y_R(D_{R_4})$
1+1	0.31365(7)	0.7870(2)	1.2603(4)	1.7338(6)	0.4733(2)	0.4734(2)	0.4735(3)
	0.47313(4)	1.1057(2)	1.7386(3)	2.3714(2)	0.63267(6)	0.63275(8)	0.63274(8)
2+1	0.23081(7)	0.9123(5)	1.5937(9)	2.275(2)	0.6815(4)	0.6814(5)	0.6816(7)
	0.1154(6)	0.6813(3)	1.2472(3)	1.8133(3)	0.56607(6)	0.56608(7)	0.56610(6)
3+1	0.1073(8)	0.9524(6)	1.7974(5)	2.643(1)	0.8449(6)	0.8445(9)	0.845(1)
	-0.2102(5)	0.3160(7)	0.8426(5)	1.369(2)	0.5271(2)	0.5270(3)	0.5269(4)
4+1	0.012(3)	0.992(6)	1.962(3)	2.95(2)	0.980(7)	0.978(6)	0.976(6)
	-0.456(4)	0.049(4)	0.553(4)	1.059(7)	0.5039(4)	0.5039(5)	0.5036(8)
4+1*	0.002(2)	1.000(3)	2.01(2)	3.02(3)	1.005(8)	1.01(1)	1.003(7)
	-0.494(3)	0.006(5)	0.506(4)	1.007(5)	0.5005(3)	0.5000(3)	0.4996(4)
5+1	0.0003(6)	0.9994(6)	2.0002(4)	2.999(3)	0.9992(6)	0.9991(8)	1.000(2)
	-0.498(1)	0.002(2)	0.502(2)	1.002(2)	0.4996(6)	0.4996(7)	0.4996(6)

TABLE XII: Result for critical exponents from the dimensionless ratios in Eq.(32). Hereby,  $y_A(D_{A_k})$  ( $A=N, R$ ;  $k=2, 3, 4$ ) is from the fit of  $D_{A_k}$ . The symbol “\*” means that the logarithmic corrections are taken into account for  $d = 4$ .

$p_c$ . In comparison with the existing results, our estimates about  $p_c$  is comparable or somewhat better for  $d = 1$  and is much more precise for  $d > 1$  dimensions. For many models, the  $p_c$  estimates are presented for the first time. This suggests that, as equilibrium case, dimensionless ratios are also useful in locating the transitions in non-equilibrium systems.

Based on the numerical data, the conditional probability distribution of the wet-site number  $N(t)$  and of the revised gyration radius  $R(t)$  at criticality is conjectured, which only involves one critical exponent. By means of finite-size scaling, we determine the critical exponents to a high precision, which can serve as a testing ground for future study of systems in the directed-percolation universality class.

d+1	$\beta$	$\nu_{\parallel}$	$\nu_{\perp}$	$z$	$\theta$	$\delta$
1+1(Present)	0.2765(2)	1.7343(6)	1.0972(6)	1.5806(2)	0.31365(7)	0.15944(2)
Ref. [20]	0.276486(8)	1.733847(6)	1.096854(4)	1.580745(10)	0.313686(8)	0.159464(6)
2+1(Present)	0.5812(6)	1.2890(7)	0.7297(5)	1.7665(2)	0.23081(7)	0.4509(2)
Ref. [24, 39]	0.584(4)	1.295(6)	0.734(4)	1.76(3)	0.230	0.451
Ref. [25]				1.7666(10)	0.2303(4)	0.4509(5)
3+1(Present)	0.817(2)	1.107(2)	0.583(2)	1.8972(8)	0.1073(8)	0.7382(5)
Ref. [40]	0.81(1)	1.105(5)	0.581(5)	1.90(1)	0.12	0.73
4+1(Present)	0.976(8)	1.017(3)	0.512(2)	1.985(2)	0.012(3)	0.960(5)
4+1(Present)*	0.996(3)	1 (fixed)	0.5005(5)	1.998(2)	0.002(2)	0.996(3)
5+1(Present)	0.9980(9)	1 (fixed)	0.4998(8)	2.001(3)	0.0003(6)	0.9980(9)
M.F.	1	1	$\frac{1}{2}$	2	0	1

TABLE XIII: Final estimate of critical exponents in 1+1 to 5+1 dimensions.

## VI. ACKNOWLEDGMENTS

J.F.W acknowledges the useful discussion with Wei Zhang. The simulation is performed on the ITS sever of New York University. This work is supported by the National Nature Science Foundation of China under Grant No. 10975127 and 91024026, and the Chinese Academy of Sciences. J.F.W and Y.J.D also acknowledge the Specialized Research Fund for the Doctoral Program of Higher Education under Grant No. 20103402110053.

- 
- [1] S. R. Broadbent and J. M. Hammersley, Proc. Camb. Phil. Soc. **53**, 629 (1957).
- [2] D. Mollison, J. Roy. Stat. Soc. B **29**, 283 (1977).
- [3] J. P. Bouchaud and A. Georges, Phys. Rep. **195**, 127 (1990).
- [4] S. Havlin and D. Ben-Avraham, Adv. Phys. **36**, 695 (1987).
- [5] E. V. Albano, J. Phys. A **27**, L881 (1994).
- [6] H. Hinrichsen, Adv. Phys **49**, 815 (2000).
- [7] G. Ódor, Rev. Mod. Phys **76**, 663 (2004).
- [8] H. Hinrichsen, Braz. J. Phys **30**, 69 (2000).
- [9] H. Hinrichsen, Physica A **369**, 1 (2006).
- [10] H. K. Janssen, Z. Phys. B **42**, 151 (1981).
- [11] P. Grassberger, Z. Phys. B **47**, 365 (1982).
- [12] K. A. Takeuchi, M. Kuroda, H. Chaté, and M. Sano, Phys. Rev. Lett **99**, 234503 (2007).
- [13] K. A. Takeuchi, M. Kuroda, H. Chaté, and M. Sano, Phys. Rev. E **80**, 051116 (2009).
- [14] J. Blease, J. Phys. C: Solid State Phys **10**, 917 (1977).
- [15] J. W. Essam, A. J. Guttmann and K. De’Bell, J. Phys. A: Math. Gen **21**, 3815 (1988).
- [16] R. J. Baxter and A. J. Guttmann, J. Phys. A: Math. Gen **21**, 3193 (1988).
- [17] D. Ben-Avraham, R. Bidaux and L. S. Schulman, Phys. Rev. A **43**, 7093 (1991).
- [18] I. Jensen and A.J. Guttmann, J. Phys. A: Math. Gen **28**, 4813 (1995).
- [19] I. Jensen, J. Phys. A **29**, 7013 (1996).
- [20] I. Jensen, J. Phys. A **32**, 5233 (1999).
- [21] S. Lúbeck and R. D. Willmann, J. Phys. A: Math. Gen **35**, 10205 (2002).
- [22] I. Jensen, J. Phys. A: Math. Gen **37**, 6899 (2004).
- [23] P. Grassberger, J. Phys. A: Math. Gen **22**, 3673 (1989).
- [24] P. Grassberger and Y. C. Zhang, Physica A **224**, 169 (1996).
- [25] E. Perlsman and S. Havlin, Europhys. Lett **58**, 176 (2002).
- [26] J. Adler, J. Berger, J.A.M.S. Duarte and Y. Meir, Phys. Rev. B **37**, 7529 (1988).
- [27] S. Lúbeck and R. D. Willmann, J. Stat. Phys **115**, 1231 (2004).
- [28] P. Grassberger, J. Stat. Mech. Th. Exp. 2009: P08021.
- [29] K. Binder, Z. Phys. B: Condens. Matter **43**, 119 (1981).

- [30] H. W. J. Blóte, L. N. Shchur, and A.L. Talapov, *Int. J. Mod. Phys. C* **10**, 1137 (1999).
- [31] Y. J. Deng and H. W. J. Blóte, *Phys. Rev. E* **68**, 036125 (2003).
- [32] H. W. J. Blóte and Y. J. Deng, *Phys. Rev. E* **66**, 066110 (2002).
- [33] Y. J. Deng and H. W. J. Blóte, *Phys. Rev. E* **72**, 016126 (2005).
- [34] P. Grassberger, *Phys. Rev. E* **67**, 036101 (2003).
- [35] P. Grassberger, *Phys. Rev. E* **79**, 052104 (2009).
- [36] H. K. Janssen, O. Stenull, *Phys. Rev. E* **69**, 016125 (2004).
- [37] H. K. Janssen, U. C. Täuber, *Ann. Phys. (N.Y.)* **315**, 147 (2005).
- [38] C. Kurrer and K. Schulten, *Phys. Rev. E* **48**, 614 (1993).
- [39] C. A. Voigt and R. M. Ziff, *Phys. Rev. E* **56**, R6241 (1997).
- [40] I. Jensen, *Phys. Rev. A* **45**, R563 (1992).